Fracture Failure Analysis of Rear Axle Suspension Control Arm in Automobile

ZhengYuan.Li [1,*], Yang.Gao[1], QingHe.Xiao [1,*]

[1] University Science and Technology Liaoning, College of applied technology, Anshan, China
     gy5520444@sina.com

*   Correspondence: lzyzhengyuan@ustl.edu.cn; xqh891024@126.com

Abstract: Fracture failure occurred in the control arm of the rear axle suspension of a certain vehicle model. To determine the root cause of the failure, comprehensive analyses were conducted, including macroscopic fracture examination, microscopic fracture analysis, microstructural characterization, and hardness testing. The results indicate that the failure was caused by the combined effects of material defects, improper manufacturing processes, and service loading conditions. The fundamental cause of the fracture lies in the initiation of microcracks at the interface between coarse Al-Fe-Si-Mn inclusions and the matrix under cyclic loading. The presence of a strength gradient induced by local segregation of Si further accelerated crack propagation along the inclusion/matrix interface. Under cyclic stress, the cracks propagated progressively through a fatigue striation mechanism and exhibited intergranular fracture in the precipitation-enriched zones along grain boundaries. Ultimately, these factors led to premature fatigue failure of the control arm.

**Keywords:** control arm; fracture analysis; fatigue striation mechanism; intergranular fracture

1. Introduction

The control arm, as a key force-transmitting and guidance component of the automotive suspension system, plays a critical role in determining the suspension's strength and stiffness performance. This core component not only provides the necessary multi-directional support for the wheels but also transmits external forces from the wheels to the vehicle body when subjected to various complex loads including static loads, high-amplitude/broadband road impacts, and medium-to-low frequency braking and steering cycles. It ensures that the wheels follow a controlled trajectory [1–3] and is crucial to the overall safety of the vehicle. Therefore, the control arm should have sufficient strength, rigidity, and good impact resistance and reliability [4-6].

Guan Yongjian et al. [7] analyzed the causes of early fracture in the control arm of a passenger car and proposed an improvement plan based on their findings. Wei Xianyi et al. [8] found that weld cold cracking can lead to early failure of the control arm, and demonstrated that improved processes can reduce this risk. Zhang Xin et al. [9] used CAE analysis to optimize the control arm structure, aiming to reduce stress concentration and solve the fracture problem. Yuan Chao et al. [10], through physical and chemical analysis combined with CAE simulation, found that the forged aluminum control arm of a certain vehicle model contained a folding defect

caused by misalignment during the forging and bending process. This defect led to fracture failure, and the authors proposed corrective measures.

In conclusion, the performance of the automotive suspension control arm is directly related to the safety of the vehicle and its occupants. Therefore, it is necessary to have an in-depth discussion on the causes of control arm breakage [11-12]. This study focuses on the fractured aluminum alloy control arm of the rear axle suspension from a specific vehicle brand (Figure 1). Detailed analyses of the material's chemical composition, fracture morphology, microstructure, and hardness were conducted. The findings aim to provide a theoretical basis for the optimization of material selection, structural design, and manufacturing processes for rear axle suspension control arms in the automotive industry. Meanwhile, it helps to improve the material failure theory system and deepen the research on the relationship between microstructure and material properties.
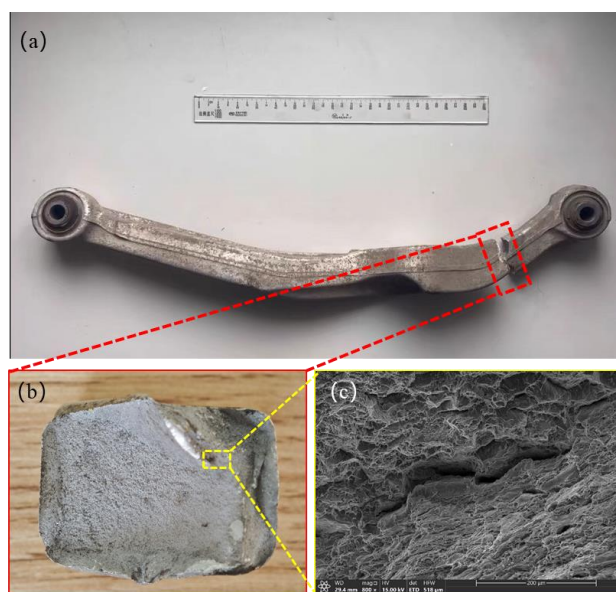
Figure 1. Fracture Location of the Elbow and Microstructure of the Fracture Surface

2. Experimental Results

2.1 Chemical Composition Analysis

The chemical composition of the aluminum alloy control arm from the rear axle suspension was analyzed using a Zeiss Gemini 300 field emission scanning electron microscope equipped with an EDS energy spectrometer. The results are presented in Table 1. The composition meets the technical specifications for A356-T6 aluminum alloy.

Table 1. Chemical composition of alloy

Element	Weight / %
Al	Bal.
Ti	0.03~0.10
Cr	0.15~0.20
Fe	0.20~0.50
Cu	0.40~0.50
Si	0.8~1.5
Mn	0.40~0.90

2.2 Hardness Test Analysis

To evaluate the uniformity of the mechanical properties of the aluminum alloy control arm from the rear axle suspension, a Vickers hardness test was performed using a load of HV0.2. The test was conducted with an XHB-3000 digital Vickers hardness tester. Ten different positions were selected on the sample for measurement. The hardness test results are shown in Table 2. The hardness values at the ten points varied by less than 10 HV, indicating relatively uniform surface hardness. This result is characteristic of a homogeneous composite material. No local softening or hardening was observed.

Table 2. Hardness Test Results

Positions	Hardness / HV
1	136.7
2	133.8
3	134.0
4	134.1
5	137.6
6	143.8
7	138.4
8	138.7
9	141.8
10	136.7
average	137.56

2.3 Fracture surface observation

### 2.3.1 Fracture macroscopic observation

The macroscopic morphology of the fracture surface is shown in Figure 2. The overall appearance is bright and metallic, with no evident signs of plastic deformation. Clear fatigue striations are observed, indicating a typical fatigue fracture. Based on the propagation direction of the fatigue striations, the fracture surface can be divided into three distinct zones: the fatigue initiation zone (a), the final fracture zone (b), and the fatigue crack propagation zone (c).
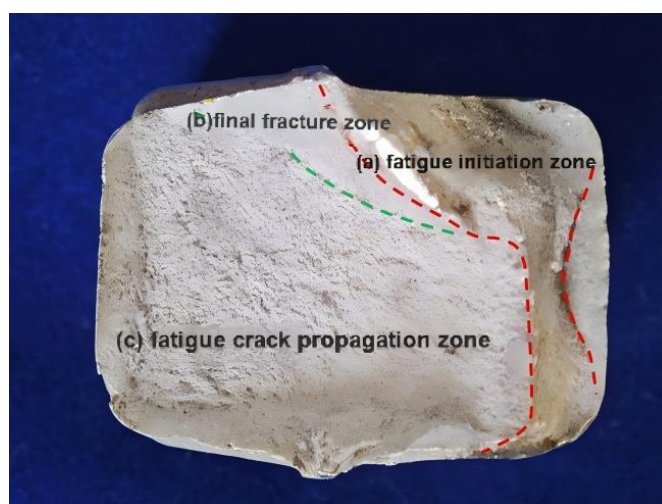
Figure 2. Macroscopic morphology of the fracture surface.

2.3.2 Fracture microscopic observation

Microscopic examination of the fracture surface was conducted using the Zeiss Gemini 300 field emission scanning electron microscope to reveal the underlying fracture mechanisms and failure processes of the aluminum alloy component. The observations confirmed characteristic features of fatigue fracture, with the fracture surface clearly divided into three distinct regions based on morphological differences: the fatigue initiation zone, the final fracture zone, and the crack propagation zone (Figure 3).
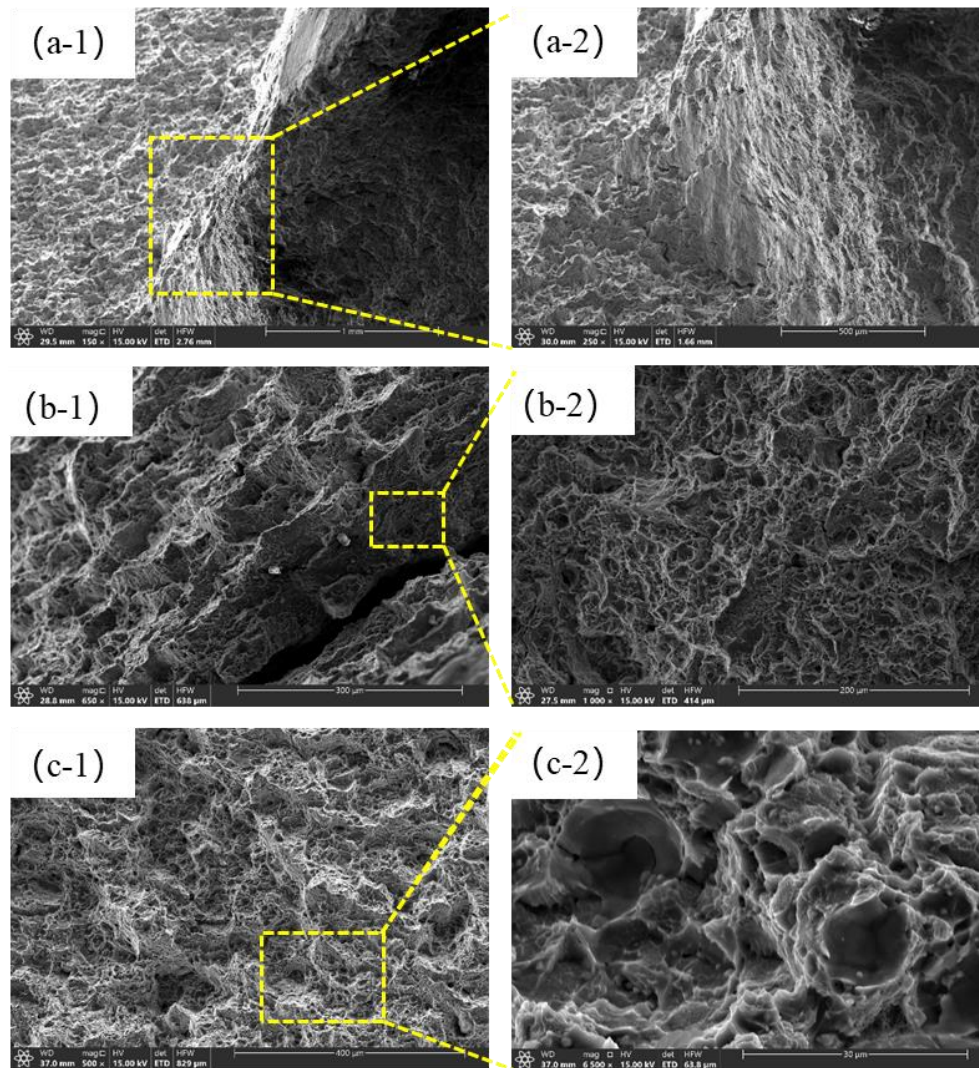
Figure 3. Fracture Surface morphology of the fracture surface.

In the fatigue initiation zone (corresponding to Figures a-1 and a-2), two distinct crack initiation sites were identified. The first originated from a relatively large surface pit, approximately 0.5 mm in depth and 0.8 mm in width. SEM images revealed fatigue striations radiating toward the center of this defect. The second crack initiation site was associated with a machining-induced tool mark, approximately 0.4 mm in depth. A clear fatigue edge line can be seen radiating outward from the root of the tool mark, located in the R-angle transition zone of the key force-bearing part of the component.

The microscopic morphology of the final fracture zone (corresponding to Figures b-1 and b-2) is primarily characterized by flat cleavage steps and typical river patterns. In some localized areas, small dimples are also observed. This brittle fracture morphology dominates a large portion of the overall fracture surface.

The crack propagation zone (corresponding Figure c-1 and c-2) shows typical fatigue fracture characteristics, including obvious cleavage patterns, fatigue bands about (2-3) μm apart, and multiple interleaved secondary cracks.

2.4 Microstructure observation

The axial profile perpendicular to the cross-section was examined using a Zeiss Gemini 300 field emission scanning electron microscope (FE-SEM). The samples were mechanically ground using water-based abrasive papers ranging from 150# to 2000#, then polished with 2.5 μm diamond paste, and finally chemically etched using a reagent composed of 1 % HF, 1.5 % HCl, 2.5 % HNO_3, and 95 % H_2O.

The observations revealed a significant network of secondary cracks in the crack initiation area (Figure 4). As shown in Figure 4-C, representative secondary cracks reach lengths of up to 15 μm. The crack propagation path exhibits a mixed fracture mode, combining intergranular and transgranular features.

More importantly, Figure 4-D reveals white precipitated phases distributed along the crack path. The interfacial energy between these second-phase particles with sizes ranging from 200 nm 500 nm and the matrix is much higher than the grain boundary energy of the Al matrix. These brittle second-phase particles have a weak bonding force with the matrix, intensifying the stress concentration within the grains and at the grain boundaries, providing a source for crack initiation. Microcracks tend to form and propagate around them, causing fracture to occur prematurely. In Figure 4-B, a void triplet is observed with dimensions of 5.8 μm, 7.2 μm, and 6.1 μm.
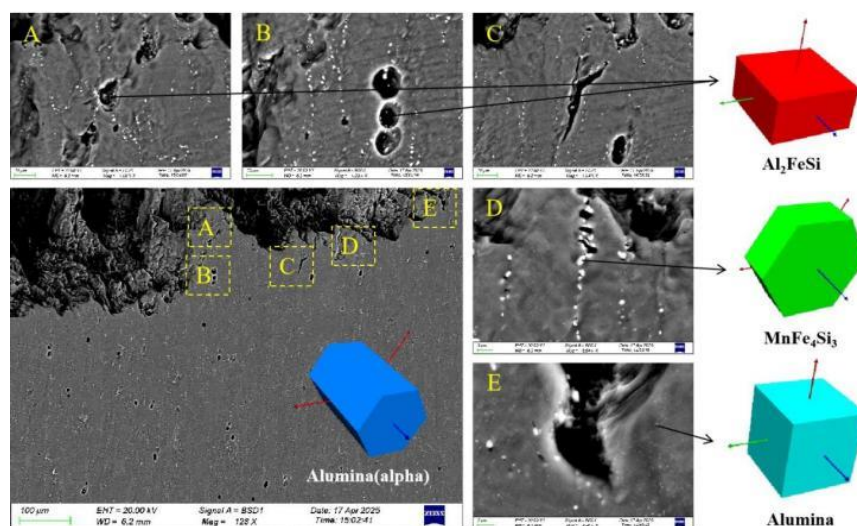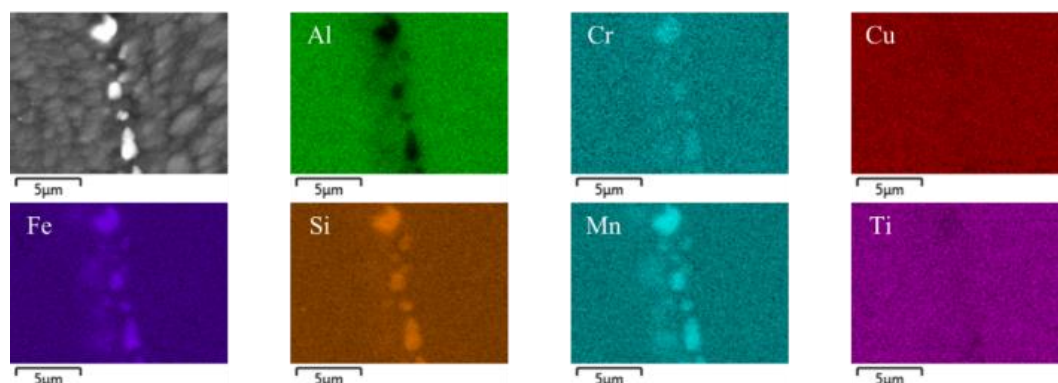

Figure 4. Fracture Longitudinal Section Morphology of the fracture surface.

EDS line scan observation (Figure 5) revealed a compositional gradient of Si content extending from the inclusion toward the aluminum matrix. Within a 2 μm distance from the interface, the Si content decreased gradually from 4.2 wt.% to 2.8 wt.%.EDS area scan analysis of the crack initiation zone (Figure 6) revealed significant elemental segregation of Si and Mn. A Si-enriched band approximately 2.5 μm in width was observed along both sides of the crack path, with a local Si concentration reaching up to 5.2 wt.%, compared to an average Si content of only 1.1 wt.%.
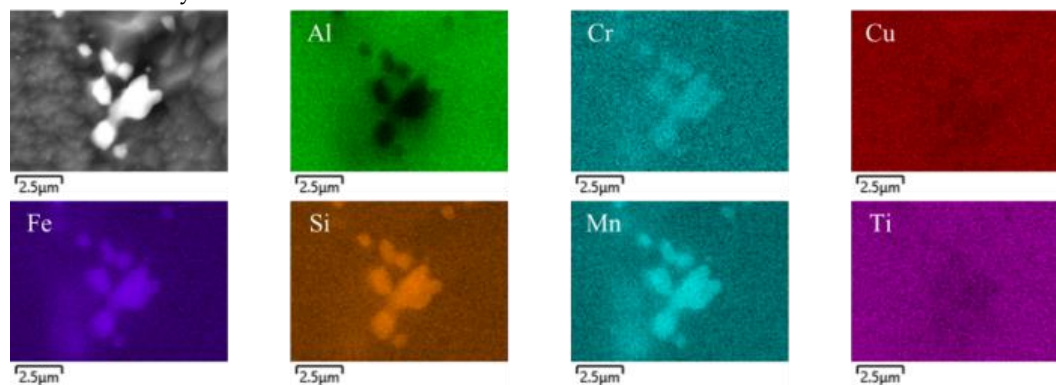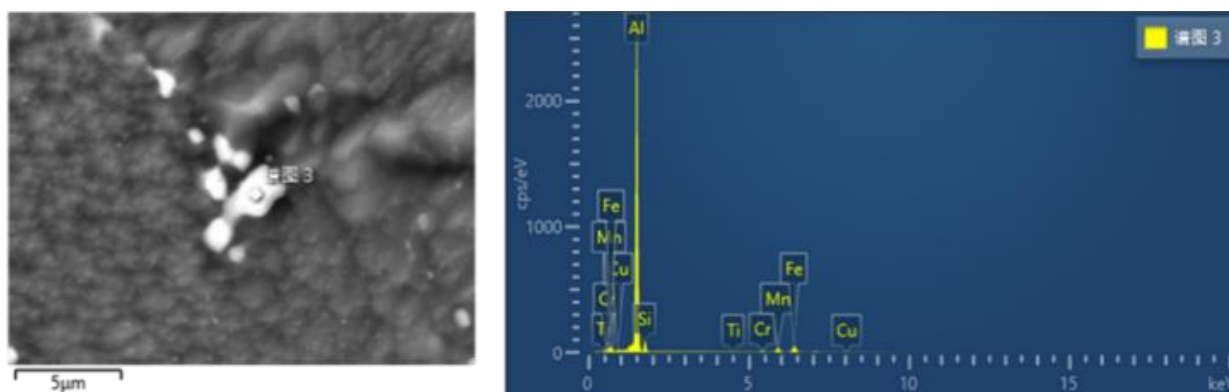

Figure 5. EDS Maps of Area Scans of Precipitate Phases on the Fracture Longitudinal Section

Figure 6. EDS Maps of Precipitate Phases at the Crack on the Fracture Longitudinal Section

Point EDS analysis was performed on precipitates located near the crack path, and the compositional results indicate that these precipitates are primarily silicide phases. According to the elemental quantification from point scan EDS analysis (Figure 7, Table 3), these silicide particles are predominantly identified as α-$Al_2(Fe\text{-}Si)$ phases, containing alloying elements such as Fe and Si.

Figure 7. EDS Maps of Precipitate Phase Point Scans on Fracture Longitudinal Section

Table 3. Composition of Precipitate Phase Point Scans

Element	Weight / %	Atomic / %
Al	78.23	85.19
Ti	6.36	6.66
Cr	0.04	0.03
Fe	0.94	0.53
Cu	5.26	2.81
Si	8.45	4.45
Mn	0.70	0.32
Total	100.00	100.00

After mechanical grinding and mechanical polishing, the sample is subjected to electrolytic polishing at room temperature. The ratio of the electrolytic polishing solution is 20 ml of H_2SO_4+80 ml of CH_3OH, and polishing is carried out for 25 seconds at a voltage of 25 V. EBSD analysis of the samples was performed using a Zeiss Gemini 300 field emission scanning electron microscope equipped with an Oxford Symmetry probe, the operating voltage was 20 kV during the test, and the sample surface was 70° from the horizontal direction. The step size of the EBSD surface distribution map is determined by the grain size or the second phase size in the sample, and is usually 1/5 to 1/10 of the minimum feature size required for analysis. The EBSD data obtained

were processed through the TSL-OIM Analysis version 8.0 software. Inverse Pole Figures (IPF) and Kernel Average Misorientation (KAM) of the longitudinal section of the fracture were obtained (Figure 8).
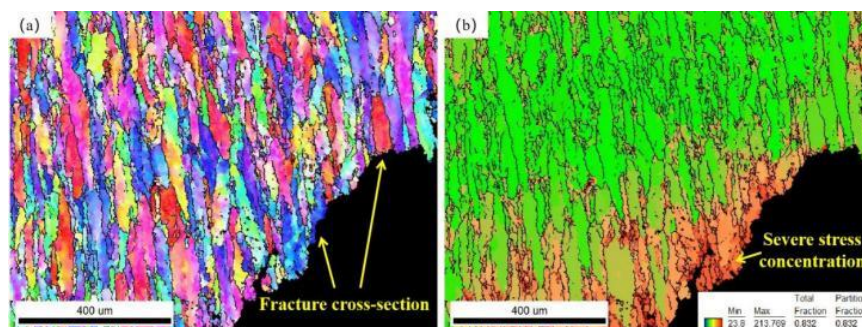

Figure 8. Fracture Longitudinal Section IPF and KAM Maps

3. Analysis and Discussion

Based on the results of chemical composition and hardness testing, it can be concluded that both the chemical composition and hardness of the control arm meet the relevant technical specifications. No visible pores, slag inclusions, or other metallurgical defects were observed on the sample surface, and there is no evidence of local softening or hardening. Therefore, it can be inferred that neither the base material nor the matrix strength are the primary causes of the fracture failure observed in the control arm. Special attention should instead be given to other potential contributing factors, such as macroscopic stress concentrations, cyclic fatigue loading, and the influence of silicide precipitates.

Based on the fracture macroscopic observation, it can be concluded that the control arm fracture originated from the surface, and the crack propagation zone presented a conchoidal arc, that is, fatigue sheen. The ductility of the aluminum alloy led to a relatively shallow sheen. The final fracture zone is rough and uneven, with a large area, indicating significant overload at the final fracture. Further analysis of the Fracture microscopic reveals that, the characteristic of the fatigue arc converging towards the center at the pit defect in the fatigue initiation zone reveals severe stress concentration, making it a preferred crack nucleation point under alternating loads.

The cracks derived from the machining tool marks and their radial fatigue edges fully demonstrate the crucial influence of surface machining quality on fatigue performance. Especially the tool marks located in the transition zone of the R-angle, their formation may be related to the "tool shaking" phenomenon, significantly reducing fatigue life. The morphological characteristics of the crack propagation zone reflect that the component has been subjected to high stress amplitude and low-frequency cyclic loads. Multiple secondary cracks further confirm that the material exhibits obvious brittle features during fatigue propagation. The fatigue band spacing can be used to quantitatively evaluate the crack propagation rate and stress level.

The final fracture zone is characterized by the morphology of cleavage steps and river patterns, combined with their relatively large proportion, indicating that rapid brittle fracture occurred when the crack reached the critical size. The river pattern indicates the direction of crack propagation, and the height of the cleavage steps reflects the brittleness degree of the material. Comprehensive analysis indicates that the fracture of this aluminum alloy component is a typical multi-source fatigue fracture and fails in a brittle manner. The main reasons include: Stress concentration caused by surface quality defects (pits and tool marks) (the most critical factor), insufficient toughness of the material itself, and alternating loads with high stress amplitudes.

Microstructural analysis indicates that the fundamental cause of fracture failure in this aluminum alloy lies in an interface-dominated, multi-level damage mechanism induced by coarse silicide phases and elemental segregation. The siliconized phases of α-$Al_2(Fe\text{-}Si)$ and $(Fe,Mn)_4Si_3$ with a size exceeding 10 μm distributed the crack initiation zone. Due to the performance mismatch such as low interfacial binding energy with the matrix, significant crystal structure differences, and a thermal expansion coefficient difference of approximately

$\Delta\alpha\approx7\times10^{-6}$/K, the damage is driven by a dual action under cyclic loading. It not only directly induces the nucleation of microcracks that exceed 90 % of crack sources as brittle particles but also promotes interfacial dissociation to form nano-micropores due to the thermal mismatch stress. These nano-micropores aggregate and grow into triplet voids ranging from 5.8 μm to 7.2 μm through dislocation slip mechanisms, resulting in a loss of 35 % of the effective bearing area of the material.

Additionally, EDS scan analysis confirmed that elemental segregation significantly weakens the material: silicon concentration decreases from 4.2 wt.% at the inclusion–matrix interface to 2.8 wt.% beyond 2 μm into the matrix, forming a localized under-aged zone. Silicon-rich bands approximately 2.5 μm wide were observed along both sides of the crack path, with local silicon concentrations reaching up to 5.2 wt.%, compared to an average matrix value of only 1.1 wt.%. These zones, in conjunction with manganese enrichment, form a low-strength path that facilitates crack propagation. EBSD analysis further revealed interfacial strain concentration effects. Based on IPF and KAM plots, the dislocation density at the silicide/matrix interface was found to be 3 to 8 times higher than that of the surrounding matrix. This local lattice rotation and dislocation proliferation, induced by the compositional gradient, may reinforce the interface structurally, but ultimately lead to a significant reduction in fracture toughness.

Comprehensive analysis indicates that the failure of the aluminum alloy control arm resulted from a combination of material defects, improper manufacturing processes, and in-service loading conditions. This fracture analysis provides important insights for the field of automotive lightweight engineering by revealing the underlying failure mechanisms of aluminum alloy control arms. The findings offer a theoretical foundation for the optimized design of critical chassis components. Specifically, the key features of interface damage under high-stress conditions have been identified and can serve as essential parameters for life prediction models of similar parts, enabling more accurate service life assessments.

Promote the transformation of the acceptance standards for automotive parts from a single performance judgment index to a multi-dimensional collaborative judgment of "surface integrity - microstructure - composition uniformity", opening up a new path for the engineering practice of high-reliability lightweight chassis systems.

4. Conclusions

In conclusion, the failure mechanism in the crack initiation zone can be described as follows: under cyclic loading, microcracks first nucleated at the interface between coarse Al-Fe-Si-Mn inclusions and the aluminum matrix. The presence of a strength gradient induced by local Si segregation facilitated rapid crack propagation along the inclusion/matrix interface. Subsequently, under continued cyclic stress, the crack propagated progressively through the formation of fatigue striations, accompanied by intergranular fracture along precipitate-enriched grain boundary zones. This multi-mode crack initiation and propagation process ultimately led to premature fatigue failure of the component.

Based on the above analysis, several improvement measures are recommended: First, the machining process parameters should be optimized, with strict control over surface quality, especially in critical load-bearing areas, to ensure surface integrity. Second, surface treatment techniques such as shot peening may be considered to improve the residual stress state at the surface. Third, in terms of material selection, it is advisable to use aluminum alloys with higher fracture toughness or to optimize the heat treatment process of the current alloy to enhance ductility. Fourth, the heat treatment protocol should be refined to promote sufficient elemental diffusion and eliminate strength gradients. A well-designed heat treatment schedule can also facilitate the spheroidization of silicide phases and reduce stress concentrations around precipitates. Lastly, from a structural design perspective, increasing the fillet radius in transition regions and optimizing load-bearing geometry can effectively reduce stress concentration. These improvement strategies should be evaluated and selected based on actual service conditions and cost considerations to ensure both performance and manufacturability.

References

[1]   Y. P. Wei, Q. Yang, T. R. Liu, et al., "Lightweight Design and Verification of Carbon Fiber Composite Control Arm (碳纤维复合材料控制臂的轻量化设计与验证)," Composites Science and Engineering, no. 9, pp. 74–78, Sep. 2019. (in Chinese). [Online]. Available: https://link.cnki.net/kns/defaultresult/index

[2]   L. Han, "Forming process of 6082 aluminum alloy control arm for automotive suspension (汽车悬架 6082 铝合金控制臂成形工艺)," Industrial Heating, vol. 48, no. 5, pp. 1–3, Oct. 2019. (in Chinese). [Online]. Available: https://link.cnki.net/kns/defaultresult/index

[3]   R. S. Tong, "Design optimization of automotive aluminum alloy control arms (汽车铝合金控制臂设计优化)," Foundry Technology, vol. 39, no. 11, pp. 2519–2521, 2528, Nov. 2018. (in Chinese). [Online]. Available: https://oversea.cnki.net/kns/defaultresult/index

[4]   B. K. Gao, Y. Q. Shi, K. Jin, et al., "The influence of mold temperature on the microstructure of forged aluminum alloy control arms (模具温度对锻造铝合金控制臂组织的影响)," Forging & Stamping Technology, vol. 45, no. 5, pp. 38–42, May 2020. (in Chinese). [Online]. Available: https://oversea.cnki.net/kns/defaultresult/index

[5]   K. Cui, Y. T. Ma, C. L. Fu, et al., "Research on Heat Treatment Process of 6082 Aluminum Alloy Control Arm (6082 铝合金控制臂热处理工艺研究)," Automobile Technology & Material, no. 7, pp. 42–44, 48, Jul. 2017. (in Chinese). [Online]. Available: https://oversea.cnki.net/kns/defaultresult/index

[6]   Z. J. Luo, W. Li, Y. C. Yao, et al., "Failure Analysis for Automobile Control Arm (控制臂失效分析)," Equipment Manufacturing Technology, no. 12, pp. 51–53, Dec. 2014. (in Chinese). [Online]. Available: https://oversea.cnki.net/kns/defaultresult/index

[7]   Y. J. Guan, H. J. Yin, and P. Y. Li, "Analysis and Improvement of Early Fracture of Suspension Control Arm in a Passenger Car (某乘用车悬架控制臂早期断裂原因分析及改进)," Journal of Guangxi University of Science and Technology, vol. 29, no. 3, pp. 57–61, 88, Jul. 2018. (in Chinese). [Online]. Available: https://oversea.cnki.net/kns/defaultresult/index

[8]   X. Y. Wei, et al., "Failure Analysis of the Low Arm of Automobile (汽车下摆臂断裂失效分析)," Automobile Parts, no. 7, pp. 97–99, Jul. 2018. (in Chinese). [Online]. Available: https://oversea.cnki.net/kns/defaultresult/index

[9]   X. Zhang and Z. B. Liu, "Analysis and optimization of lower front control arm fracture in a vehicle model (某车型前悬下摆臂断裂问题分析与优化)," Highway and Automobile Transportation, no. 1, pp. 11–12, Jan. 2022. (in Chinese). [Online]. Available: https://oversea.cnki.net/kns/defaultresult/index

[10]   C. Yuan, H. W. Li, Q. Ma, et al., "Failure Analysis of Forged Aluminum Control Arm (锻铝控制臂失效分析)," Forging & Stamping Technology, vol. 46, no. 6, pp. 72–76, 132, Jun. 2021. (in Chinese). [Online]. Available: https://oversea.cnki.net/kns/defaultresult/index

[11]   B. Zhang, H. Chen, L. Z. Wang, et al., "Research on aluminum alloy control arm and the die design (铝合金控制臂研究及模具设计)," Die & Mould Industry, vol. 51, no. 2, pp. 69–73, Feb. 2025. (in Chinese). [Online]. Available: https://oversea.cnki.net/kns/defaultresult/index

[12]   Y. Z. You, H. Y. Zhu, G. D. Wu, et al., "Structural Performance Evaluation and Optimization Design of a Passenger-Vehicle Front (某乘用车前悬下控制臂结构性能评估与优化设计)," Journal of East China Jiaotong University, vol. 41, no. 6, pp. 106–111, Dec. 2024. (in Chinese). [Online]. Available: https://oversea.cnki.net/kns/defaultresult/index

https://doi.org/10.64486/m.65.1.3